



Accepted Article

Title: Photoinduced Nonadiabatic Decay-guided Molecular Motor Triggers Effective Photothermal Conversion for Hyperthermia Cancer Therapy

Authors: Jen-Shyang Ni, Xun Zhang, Guang Yang, Tianyi Kang, Xiangwei Lin, Menglei Zha, Yaxi Li, Lidai Wang, and Kai Li

This manuscript has been accepted after peer review and appears as an Accepted Article online prior to editing, proofing, and formal publication of the final Version of Record (VoR). This work is currently citable by using the Digital Object Identifier (DOI) given below. The VoR will be published online in Early View as soon as possible and may be different to this Accepted Article as a result of editing. Readers should obtain the VoR from the journal website shown below when it is published to ensure accuracy of information. The authors are responsible for the content of this Accepted Article.

To be cited as: *Angew. Chem. Int. Ed.* 10.1002/anie.202002516

Link to VoR: <https://doi.org/10.1002/anie.202002516>

Photoinduced Nonadiabatic Decay-guided Molecular Motor Triggers Effective Photothermal Conversion for Hyperthermia Cancer Therapy

Jen-Shyang Ni,[†] Xun Zhang,[†] Guang Yang, Tianyi Kang, Xiangwei Lin, Menglei Zha, Yaxi Li, Lidai Wang, and Kai Li*

Abstract: Photothermal agents, which can release nonradiative heat by strongly twisted intramolecular charge transfer (TICT) state and/or molecular motions in aggregates, have been implemented in photothermal therapy for treating diseases. To achieve enhanced nonradiative decay, long alkyl-chains and bulky substituents have been proposed to be introduced into the large conjugation structure, which always require complicated synthetic procedures. Thus, it remains highly challenging to strategically explore small molecule-based photothermal agents with high photothermal conversion efficiency (PTCE). Herein, we adopt a double bond-based molecular motor concept to develop a new class of small photothermal agents to break the current design bottleneck. As the double-bond is twisted by strong TICT upon irradiation, the excited agents can deactivate nonradiatively through the conical intersection (CI) of internal conversion, which is called as photoinduced nonadiabatic decay. Such agents thus possess a high PTCE of ~90.0%, facilitating low-temperature photothermal therapy in the presence of a heat shock protein 70 inhibitor. In addition, the behaviors and mechanism of NIR laser-triggered molecular motions for generating heat via the nonradiative CI pathway have been further understood by theoretical and experimental evidence, providing a feasible design principle to synthesize highly efficient photothermal and photoacoustic agents.

Photothermal therapy (PTT) using near-infrared (NIR) light-absorbing agents to locally generate heat for tumor ablation has received considerable interest in recent years.^[1] Taking advantage of the minimal invasiveness, convenient operation, low toxicity and quick recovery, PTT using NIR laser-triggered photothermal agents has been intensively investigated in the field of phototheranostics.^[2] To obtain ideal agents with high photothermal conversion efficiency (PTCE), one of the key points is to acquire effective nonradiative transition.^[3] In view of this, some organic small molecules based on strong twisted intramolecular charge transfer state (TICT) or intramolecular motion-induced photothermy (iMIPT) properties have been developed. However, those molecular structures usually involve long-branch alkyl-chains and/or bulky substituents to support

molecular motions in aggregates, as well as long-conjugated system to extend the absorption to NIR-region. As a result, these materials not only require complex synthesis but also encounter potential biodegradation problem when used for *in vivo* studies. Thus, the new design strategy and/or mechanism to synthesize small-molecular photothermal agents with high PTCE holds great potential to promote further biomedical applications.

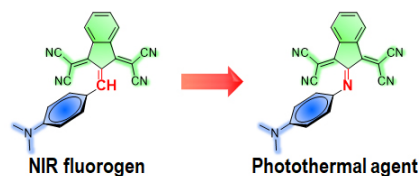
Molecular motor with an imino-rotary axis exhibits photochemical rotation around the C=N bond (C=N rotation) and thermal nitrogen-inversion (*N*-inversion) under irradiation, as a typical light-driven imine-based molecular motion (Scheme S1).^[4] Theoretically, the molecular motions via photoisomerization can release the excitation energy as heat through nonradiative pathway including conical intersection (CI), which is defined as photoinduced nonadiabatic decay (PIND). This indicates that the excited molecules can easily pass through the nonradiative CI pathway and return to the ground state as the twisted double-bond has a vertical angle (~90°). Such PIND-guided materials thus have significant potential to serve as the advanced photothermal and photoacoustic contrast agents. Inspired by this concept, we developed the molecular motor-based photothermal agents by one-step condensation synthesis, using dialkylaminophenyl-donor and 1,3-bis(dicyanomethylidene)indan (BDCl) acceptor bridged by a imino-double bond (Scheme S2).

In this work, we first synthesized a pair of imino- and vinyl-based molecular motors (Scheme 1). In comparison with the vinyl-based molecular motor (CCTI; Figure S1), the imino-based one has almost no fluorescence in either solution or solid state, which is attributed to easier intramolecular motions via double-bond torsion causing PIND effect. Interestingly, owing to the strong TICT effect, its absorption can be red-shifted to the NIR-region, further benefiting photothermal conversion under laser irradiation of 808 nm. The maximum PTCE of C6TI in the aggregation state thus can reach ~90.0%, which is greatly higher in comparison with most reported photothermal agents including ICG (Table S1).^[2b, 3a, 5] Thanks to its excellent PTCE,

[*] Prof. J.-S. Ni, X. Zhang, Dr. T. Kang, Dr. G. Yang, M. Zha, Y. Li, Prof. K. Li
Department of Biomedical Engineering, SUSTech Academy for Advanced Interdisciplinary Studies, Southern University of Science and Technology (SUSTech), Shenzhen 518055, China
E-mail: lik@sustech.edu.cn
Prof. J.-S. Ni
HKUST-Shenzhen Research Institute, Shenzhen 518057, China
Dr. X. Lin, Prof. L. Wang
City University of Hong Kong Shenzhen Research Institute, Shenzhen 518057, China

[†] These authors contributed equally to this work

Supporting information for this article is given via a link at the end of the document.



- ✓ A facile strategy for UV-vis-NIR absorbing probes
- ✓ Easier intramolecular motion around double bond
- ✓ More nonradiative decay via conical intersection
- ✓ Higher photothermal conversion efficiency at 808 nm

Scheme 1. Design strategy for highly efficient photothermal agent.

C6TI serves as a NIR-triggered PTT agent that can locally heat the tumor region to 53.4 °C and further induce complete cell necrosis (Figures S2-4). Nevertheless, the high-temperature ablation may cause heating damage of normal organs adjacent to the tumor due to heat diffuse (Figure S3).^[1d] To address this concern of side effects in conventional PTT, we employed a heat shock protein 70 (HSP70) inhibitor, apoptozole (Apo), that can against thermotolerance of tumor cells upon laser irradiation. The combination of Apo and C6TI can realize synergistic PTT in the hyperthermia region (43 °C) upon laser irradiation,^[6] which actively avoided collateral damage to normal tissues in the traditional photothermal treatment at a high temperature (over 50 °C). Overall, these insights into the working mechanism of such molecular motor and its successful implementation in biomedical practice can open a new door to explore highly-effective PTT agents for advanced tasks.

First of all, the imino-molecular motor (C1TI) shows a broad absorption profile covering from visible to NIR region, peaked at 740 nm with an intense tail extended to 1000 nm (Figure 1a). Its bathochromic absorption is contributed from the electron-rich nitrogen atom and strong TICT property. The results of theoretical calculations (Figures S5-6 and Tables S2-3) reveal that the ground-state (S_0) geometries of chiral *P*- and *M*-helical C1TI molecules have similar optimized energies, oscillator strengths (f) and dihedral angles between dimethylaminophenyl-donor and BDCI-acceptor, indicating the feasibility of chiral switch in C1TI molecules upon light irradiation. In addition, the excited C1TI molecule in the strong TICT state shows an almost vertical donor-acceptor twisting behavior (87.0°), leading to the ineffective overlap of molecular orbitals with zero f value in the emissive transition.^[7] This is the reason why the C1TI molecule does not emit in solution at room temperature (298 K) (Figure 1b).

As shown by the excited-state double-bond reorganization (ESDBR) guided potential energy surface (Figure 1c),^[8] twisting around the imino-double bond can yield a highly polar TICT state and CI in the torsional angle between -10° and 0°. This reveals that the excited C1TI molecule can be efficiently deactivated to S_0/S_1 state through the CI pathway of nonradiative internal conversion, followed by the vibrational relaxation to its original S_0 state or chiral isomer (Figure 1d).^[9] The total de-excited processes are designated as PIND. By contrast, as the donor-acceptor twisting is below 87.0°, the excitons for the local excited-state (LE) of C1TI molecule can deactivate through the radiative decay pathway in the light of RIM mechanism at a low temperature of 77 K, making it emissive upon irradiation (Figure 1b).^[3c] On the contrary, it shows negligible emission at room temperature (298 K). This suggests that the imino-molecular motor (C1TI) provides an effective approach passing through photoinduced excited-state nonadiabatic process upon irradiation with NIR laser at room temperature. In addition, the nanoaggregates of C6TI substituted with the longest alkyl-chains have the highest PTCE (90.0%) in comparison to the ones with shorter alkyl-chains (C1TI, C2TI and C4TI) (Figures S7-8). According to the iMIPT mechanism,^[3c] the substituent with long alkyl-chains is conducive to molecular motions in the aggregation state.^[3b] Specifically, such PIND-guided materials thus will befittingly serve as advanced photothermal agents.

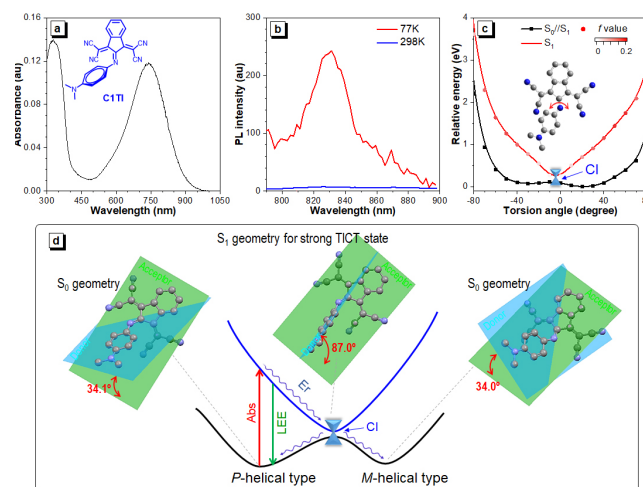


Figure 1. The photophysical properties and mechanism for imino-molecular motor (C1TI). (a) UV-vis-NIR absorption spectrum of C1TI in THF (10 μ M). (b) PL spectra of C1TI in toluene at 77 and 298 K upon excitation at 700 nm. (c) The potential energy surfaces of C1TI geometries in the excited state (S_1) as a function of the torsional angles. S_0/S_1 is the ground state (S_0) projected vertically by S_1 . (d) A proposed model of photoinduced excited-state nonadiabatic process for C1TI molecule. The inserts are its S_0 and S_1 geometries. The angles are the planar included angles between the dimethylaminophenyl-donor (blue plane) and BDCI-acceptor (green plane). Abs: absorption. CI: conical intersection. TICT: twisted intramolecular charge transfer. Er: energy relaxation. LEE: local excited-state emission.

However, through nanoprecipitation (Figures S9-10),^[10] only C6TI-loaded nanoparticles (NPs) formed stable dispersion in phosphate buffered saline (PBS) at a high concentration. By contrast, the other NPs precipitated from the suspensions due to their serious intermolecular aggregation (Figure S11). To further evaluate the photothermal performance of C6TI NPs in PBS, the solution temperatures were recorded at different concentrations under laser irradiation of 808 nm at 1 W cm^{-2} (Figure 2b). The solution temperatures with the increased concentrations of C6TI NPs from 0 to 100 $\mu\text{g mL}^{-1}$ regularly rose under laser irradiation. A highest value of 76.4 °C can be recorded at 100 $\mu\text{g mL}^{-1}$ after continuously irradiated for 8 min. In particular, it exhibited a steady-state temperature variation through 5 cycles of heating and cooling measurements (Figure 2c), whereas ICG showed serious photothermal un-stability. Additionally, the PTCE of C6TI NPs was measured to be 89.3% (Figure S12). As a result, the formulated C6TI NPs inherit the intrinsic photothermal converting ability of C6TI aggregates. On the contrary, the PTCE of ICG was only 32.0% measured under the same condition (Figure S13), owing to the fact that the excited ICG can pass the emissive pathway and return back to the ground state besides nonradiative heat release.^[11] Our non-emissive C6TI NPs thus have a significantly higher photothermal conversion performance in comparison with most recently reported organic photothermal agents.^[2b, 3b, 3c, 5d] Specifically, the excitons for the molecular motor-based materials (C6TI NPs) will mainly be deactivated through the nonradiative CI pathway to perform the perfect photothermal conversion for PTT.

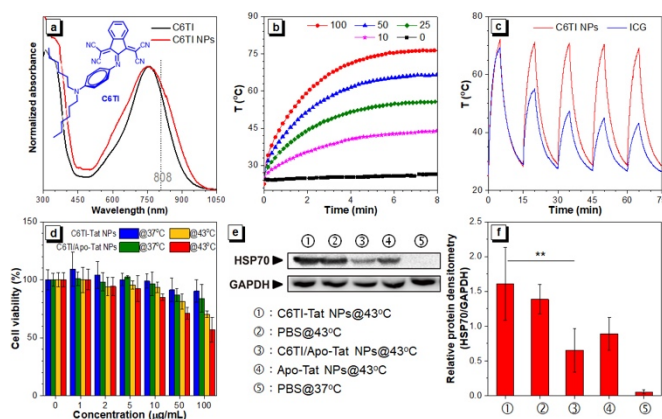


Figure 2. The photothermal properties and *in vitro* experiments of C6TI-based NPs. (a) Normalized UV-vis-NIR absorption spectra of C6TI in THF and C6TI NPs in PBS. (b) Time-dependent temperature changes of C6TI NPs in PBS with various concentrations (0–100 $\mu\text{g mL}^{-1}$) under laser irradiation (808 nm, 1 W cm^{-2}). (c) Temperature changes of C6TI NPs and ICG (100 $\mu\text{g mL}^{-1}$) over five laser-on/off cycles under 808 nm irradiation (1 W cm^{-2}). (d) Cytotoxicity of C6TI-Tat and C6TI/Apo-Tat NPs in 4T1 cells treated at 37 °C and 43 °C, respectively. (e) The HSP70 expression efficacy after different treatments as determined by western blot, and (f) the relative HSP70 quantification, using PBS-treated group as the control. Statistical significance: ** $p < 0.002$.

Although the traditional PTT with laser-induced high local temperature over 50 °C can induce complete cell necrosis in tumor tissues (Figure S4), it will also threaten the adjacent healthy cells and tissues due to the inevitable heat diffusion (Figure S3). To address this problem, we proposed an alternative approach to realize PTT for tumor ablation at a relative low temperature. C6TI/Apo-Tat NPs were prepared through co-encapsulation of the photothermal agent (C6TI) and HSP70 inhibitor (Apo),^[12] followed by conjugation with Tat peptides for cell penetrating ability^[13] (Figures S9, S10c and S14–15). The potential cytotoxicity of C6TI-based NPs was investigated by a standard cell counting kit-8 (CCK-8) assay in 4T1 cells (Figures 2d and S16). Upon co-incubation with a high concentration (C6TI at 100 $\mu\text{g mL}^{-1}$) of C6TI-based NPs at 37 °C for 24 h, no obvious cytotoxicity was detected. By contrast, through the additional PTT treatment at 43 °C for 1 h, the viability decreased to $56.8 \pm 10.6\%$ and $70.9 \pm 5.1\%$ for cells treated by C6TI/Apo-Tat and C6TI-Tat NPs, respectively. According to the cell apoptosis analysis by flow cytometry (Figure S17), the percentage of apoptotic cells increased to 23.4% upon treatment with C6TI/Apo-Tat NP at 43 °C for 1 h, whereas the control groups treated with PBS at 37 °C and 43 °C only showed slight apoptosis of 5.1% and 7.8%, respectively. This confirms that the obvious apoptosis-inducing ability originates from the suppressed thermotolerance of cancer cells by Apo. According to the result of western blot analysis (Figures 2e–f),^[14] the cells with mild thermal treatment (PBS@43 °C) displayed an up-regulated HSP70 expression in comparison with the cells in control group (PBS@37 °C), indicating that the operating temperature induced the heating stress and further up-regulated HSP70 expression.^[12a, 12b] Meanwhile, for the cells treated with Apo-loaded NPs (C6TI/Apo-Tat NP@43 °C and Apo-Tat NP@43 °C), the HSP70 expression was significantly reduced and down-regulated by the released Apo molecules

(Figure 2f). The Apo inhibitor release ratio from NPs was ca. 49.5% upon laser irradiation at 43 °C in 1 h (Figure S18). These results collectively confirm that C6TI/Apo-Tat NP is a promising nanomedicine for PTT at a relatively low temperature *via* thermoresistance suppression by HSP70 inhibitor.

Additionally, the intense NIR-absorbance of C6TI molecules can facilitate photoacoustic imaging. *In vivo* results suggest that the photoacoustic signal intensity of tumor region at 8 h post intravenous injection exhibited the maximum value (Figure S19), attributed from passive targeting effect of NPs.^[15] We thus assigned this time point for PTT treatment to realize optimized outcome. At 8 h post intravenous injection of C6TI/Apo-Tat NPs, the tumor-bearing region was irradiated by an 808 nm laser for 25 min (0.5 W cm^{-2}) and its photothermal heating profile was recorded by an IR thermal imaging system (Figure S20). The temperature of the tumor site promptly increased to 43 °C after continuous irradiation for 3 min and then remained stable. On the other hand, a higher laser power density (1 W cm^{-2}) was required to maintain the similar temperature of tumor region of mice injected with ICG/Apo-Tat NPs, due to the lower PTCE of ICG-loaded NPs (17.6%; Figures S21–22). To thoroughly investigate the efficacy of our low-temperature PTT approach, six groups were randomly established from 4T1 tumor-bearing

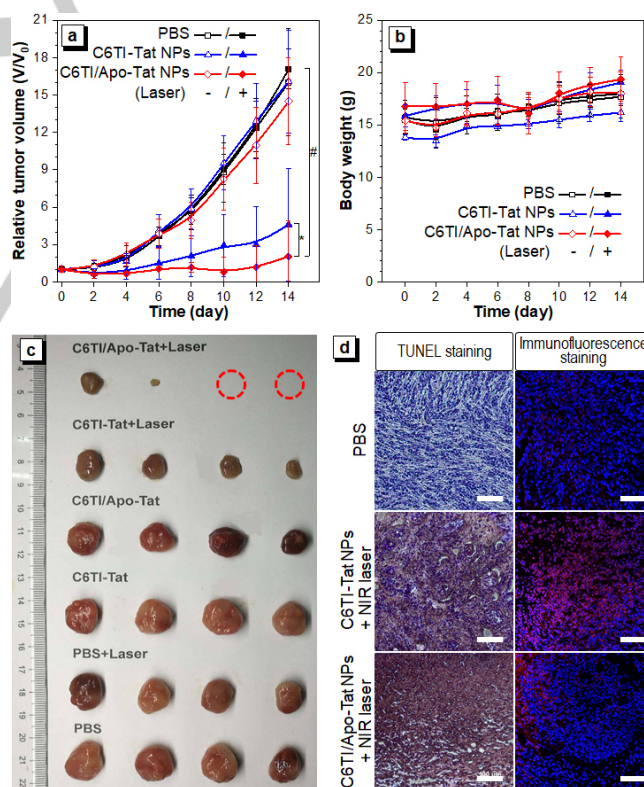


Figure 3. The *in vivo* experiments for C6TI-cored NPs in low-temperature PTT treatment. (a) Growth profiles of tumors and (b) changes of body weights after different treatments. Statistical significance: $0 < *p < 0.0005$, $0.2 < *p < 0.25$. (c) A photograph of the excised tumors from all groups. (d) TUNEL and immunofluorescence staining of tumor slices from the representative mice of different groups. Scale bars: 100 μm .

mice for the following treatments: (i) PBS, (ii) PBS with NIR laser (808 nm, 0.5 W cm⁻², 1 h), (iii) C6TI-Tat NPs, (iv) C6TI-Tat NPs with NIR laser, (v) C6TI/Apo-Tat NPs, and (vi) C6TI/Apo-Tat NPs with NIR laser. After the different treatments, their tumor sizes and body weights were periodically monitored (Figures 3a-b and S23). The tumors in PBS groups and all other groups without light irradiation grew quickly during 14 days. As a clear contrast, the tumor growth in the group treated with C6TI-Tat NPs and NIR light irradiation was restrained within day 4 post-treatment but reoccurred after day 6. The limited therapeutic efficiency is attributed to the fact that the sole PTT at 43 °C is feeble for effective tumor ablation. Among all the six groups, PTT with C6TI/Apo-Tat NPs plus laser irradiation exhibited the maximized inhibition efficiency on tumor growth, attributing to the surmounted HSP-induced thermotolerance by the released Apo as a HSP70 inhibitor to promote the tumor-killing efficacy.^[12c] Meanwhile, all treated groups did not display significant drop of body weights (Figure 3b), indicating the good tolerance of our formulations in the mice model. At day 14 post treatment, the representative photographs of excised tumors demonstrated a prominent tumor inhibition effect for C6TI/Apo-Tat NPs upon NIR laser irradiation (Figures 3c and S24). Nevertheless, this therapeutic efficacy *via* low-temperature PTT is more excellent than the reported results,^[16] owing to the fact that Apo can efficiently prevent the cytoprotective pathway of the dominant HSP factor, HSP70.^[12]

Through histological analysis of terminal deoxynucleotidyl transferase dUTP nick end labeling (TUNEL) staining, significantly large apoptotic/necrotic areas in the tumor tissues treated by the C6TI/Apo-Tat NPs and NIR laser was observed (Figure 3d). By contrast, C6TI NPs with NIR laser-treated group had evident un-killed tumor tissues while no obvious apoptotic/necrotic tissues were observed in the PBS control group. As expected, the immunofluorescence analysis results imply that the HSP expression for C6TI/Apo-Tat NPs group was dramatically inhibited with less HSP70-expression, in comparison with that for C6TI-Tat NP-treated group upon laser-irradiation. And the sample from PBS group displayed negligible HSP70-expression (Figure 3d). These results further demonstrate the high efficacy of C6TI/Apo-Tat NPs for restrained cytoprotection of HSP70, leading to enhanced apoptosis combined with tumor photothermal ablation. In the hematoxylin and eosin (H&E) stained histological images (Figure S25), no obvious pathological difference was found when comparing the major organs after individually treated. In addition, the blood circulation half-life of NPs was estimated to be ~24 h and they mainly accumulated in liver, spleen and tumor as passively targeted NPs, employing fluorescent molecule-doped NPs as the indicator (Figures S26-27). The analysis of red blood cells lysis, blood biochemistry and blood routine examinations at day 14 post NPs injection confirm that the liver and kidney functions were not affected by C6TI/Apo-Tat NPs (Figures S28-30). These results collectively confirm their good biocompatibility and circulation half-life, which are of high importance in *in vivo* therapeutic applications.

In this work, we show a significantly high-efficient photothermal conversion performance in the rationally designed PTT agents, which pass through molecular motor-induced heating release *via* PIND process under NIR-laser irradiation.

Introducing the imino-based double-bond into a strong TICT framework can achieve UV-vis-NIR absorption as well as complete nonradiative release upon laser excitation. Particularly, owing to the effective molecular motions in aggregates and complete nonradiative energy release as heat *via* CI-deactivated pathway, C6TI nanoaggregates and nanoparticles have excellent PTCE of up to ~90.0%. These results indicate the priority of C6TI as a photothermal agent than the commercial ICG and other recently reported synthetic agents (Table S1). Combined with a HSP70 inhibitor (Apo), C6TI/Apo-Tat NPs can suppress the thermotolerance of tumor cells and realize the low-temperature PTT upon laser irradiation for effective tumor ablation with minimized damage to adjacent normal tissues. Noteworthy is that we demonstrate a new strategy to develop highly-efficient small molecular photothermal agents through the excited-state PIND process, which offers a more feasible approach in comparison with the traditional design principle of PTT/PA agents by introducing long alkyl-chains and bulky substituents. As such, this investigation not only successfully introduces PIND-guided molecular motor concept to advance NIR-triggered photothermal agents, but also expands effective therapeutic systems for biomedical applications.

Experimental Section

The experimental details were described in the supporting information.

Acknowledgements

The authors are grateful to the National Natural Science Foundation of China (31870991), the Science and Technology Plan of Shenzhen (JCYJ20180306174918294), and High Level Special Funds of SUSTech (G02386301 and G02386401) for financial support. The authors also acknowledge the Center for Computational Science and Engineering at SUSTech for theoretical calculation support and SUSTech Core Research Facilities for technical support. All *in vivo* procedures have been approved by the Animal Ethics Committee of the Center for Experimental Animal Research of SUSTech, China.

Keywords: HSP70 • conical intersection • imine • photothermal therapy • NIR

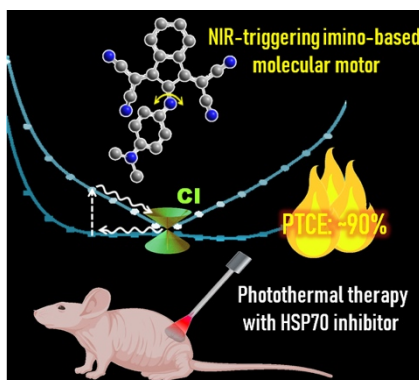
- [1] a) J. Li, K. Pu, *Chem. Soc. Rev.* **2019**, *48*, 38–71; b) Y. Liu, P. Bhattarai, Z. Dai, X. Chen, *Chem. Soc. Rev.* **2019**, *48*, 2053–2108; c) J.-S. Ni, Y. Li, W. Yue, B. Liu, K. Li, *Theranostics* **2020**, *10*, 1923–1947; d) C. J. Diederich, *Int. J. Hyperthermia* **2005**, *21*, 745–753; e) J. Li, D. Cui, Y. Jiang, J. Huang, P. Cheng, K. Pu, *Adv. Mater.* **2019**, *15*, 1905091; f) Y. Jiang, P. K. Upputuri, C. Xie, Z. Zeng, A. Sharma, X. Zhen, J. Li, J. Huang, M. Pramanik, K. Pu, *Adv. Mater.* **2019**, *31*, 1808166.
- [2] a) Y. Jiang, J. Li, X. Zhen, C. Xie, K. Pu, *Adv. Mater.* **2018**, *30*, 1705980; b) C. Liu, S. Zhang, J. Li, J. Wei, K. Müllen, M. Yin, *Angew. Chem., Int. Ed.* **2019**, *58*, 1638–1642; c) H. Wang, J. Chang, M. Shi, W. Pan, N. Li, B. Tang, *Angew. Chem., Int. Ed.* **2019**, *58*, 1057–1061; d) L. Teng, G. Song, Y. Liu, X. Han, Z. Li, Y. Wang, S. Huan, X. B. Zhang, W. Tan, *J. Am. Chem. Soc.* **2019**, *141*, 13572–13581; e) J. Li, C. Xie, J. Huang, Y. Jiang, Q. Miao, K. Pu, *Angew. Chem., Int. Ed.* **2018**, *57*, 3995–3998; f) J. F. Lovell, C. S. Jin, E. Huynh, H. Jin, C. Kim, J. L. Rubinstein, W. C. W. Chan, W. Cao, L. V. Wang, G. Zheng, *Nat. Mater.* **2011**, *10*, 324–332; g) J. Li, D.

- Cui, J. Huang, S. He, Z. Yang, Y. Zhang, Y. Luo, K. Pu, *Angew. Chem., Int. Ed.* **2019**, *58*, 12680–12687.
- [3] a) X. Li, L. Liu, S. Li, Y. Wan, J. X. Chen, S. Tian, Z. Huang, Y. F. Xiao, X. Cui, C. Xiang, Q. Tan, X. H. Zhang, W. Guo, X. J. Liang, C. S. Lee, *ACS Nano* **2019**, *13*, 12901–12911; b) S. Liu, X. Zhou, H. Zhang, H. Ou, J. W. Y. Lam, Y. Liu, L. Shi, D. Ding, B. Z. Tang, *J. Am. Chem. Soc.* **2019**, *141*, 5359–5368; c) Z. Zhao, C. Chen, W. Wu, F. Wang, L. Du, X. Zhang, Y. Xiong, X. He, Y. Cai, R. T. K. Kwok, J. W. Y. Lam, X. Gao, P. Sun, D. L. Phillips, D. Ding, B. Z. Tang, *Nat. Commun.* **2019**, *10*, 768; d) X. Cai, J. Liu, W. H. Liew, Y. Duan, J. Geng, N. Thakor, K. Yao, L.-D. Liao, B. Liu, *Mater. Chem. Front.* **2017**, *1*, 1556–1562.
- [4] D. Roke, S. J. Wezenberg, B. L. Feringa, *Proc. Natl. Acad. Sci. U. S. A.* **2018**, *115*, 9423–9431.
- [5] a) D. Gao, B. Zhang, Y. Liu, D. Hu, Z. Sheng, X. Zhang, Z. Yuan, *Theranostics* **2019**, *9*, 5315–5331; b) B. Wang, G. Feng, M. Seifrid, M. Wang, B. Liu, G. C. Bazan, *Angew. Chem., Int. Ed.* **2017**, *56*, 16063–16066; c) D. Chen, Y. Tang, J. Zhu, J. Zhang, X. Song, W. Wang, J. Shao, W. Huang, P. Chen, X. Dong, *Biomaterials* **2019**, *221*, 119422; d) J. Zhu, J. Zou, Z. Zhang, J. Zhang, Y. Sun, X. Dong, Q. Zhang, *Mater. Chem. Front.* **2019**, *3*, 1523–1531.
- [6] a) Y. Yang, W. Zhu, Z. Dong, Y. Chao, L. Xu, M. Chen, Z. Liu, *Adv. Mater.* **2017**, *29*, 1703588; b) T. Sun, X. Chen, X. Wang, S. Liu, J. Liu, Z. Xie, *Mater. Chem. Front.* **2019**, *3*, 127–136.
- [7] Y. Tu, J. Liu, H. Zhang, Q. Peng, J. W. Y. Lam, B. Z. Tang, *Angew. Chem., Int. Ed.* **2019**, *58*, 14911–14914.
- [8] a) J.-S. Ni, H. Liu, J. Liu, M. Jiang, Z. Zhao, Y. Chen, R. T. K. Kwok, J. W. Y. Lam, Q. Peng, B. Z. Tang, *Mater. Chem. Front.* **2018**, *2*, 1498–1507; b) J.-S. Ni, T. Min, Y. Li, M. Zha, P. Zhang, C. L. Ho, K. Li, *Angew. Chem., Int. Ed.* **2020**, DOI: 10.1002/anie.202001103.
- [9] D. Polli, P. Altoe, O. Weingart, K. M. Spillane, C. Manzoni, D. Brida, G. Tomasello, G. Orlandi, P. Kukura, R. A. Mathies, M. Garavelli, G. Cerullo, *Nature* **2010**, *467*, 440–443.
- [10] a) X. Qin, H. Chen, H. Yang, H. Wu, X. Zhao, H. Wang, T. Chour, E. Neofytou, D. Ding, H. Daldrup-Link, S. C. Heilshorn, K. Li, J. C. Wu, *Adv. Funct. Mater.* **2018**, *28*, 1704939; b) G. Jin, D. Mao, P. Cai, R. Liu, N. Tomczak, J. Liu, X. Chen, D. Kong, D. Ding, B. Liu, K. Li, *Adv. Funct. Mater.* **2015**, *25*, 4263–4273.
- [11] a) B. Guo, Z. Sheng, D. Hu, A. Li, S. Xu, P. N. Manghnani, C. Liu, L. Guo, H. Zheng, B. Liu, *ACS Nano* **2017**, *11*, 10124–10134; b) J. Qi, Y. Fang, R. T. K. Kwok, X. Zhang, X. Hu, J. W. Y. Lam, D. Ding, B. Z. Tang, *ACS Nano* **2017**, *11*, 7177–7188.
- [12] a) C. Liu, W. Lou, J. C. Yang, L. Liu, C. M. Armstrong, A. P. Lombard, R. Zhao, O. D. V. Noel, C. G. Tepper, H.-W. Chen, M. Dall’Era, C. P. Evans, A. C. Gao, *Nat. Commun.* **2018**, *9*, 4700; b) D. R. Williams, S. K. Ko, S. Park, M. R. Lee, I. Shin, *Angew. Chem., Int. Ed.* **2008**, *47*, 7466–7469; c) S. K. Ko, J. Kim, D. C. Na, S. Park, S. H. Park, J. Y. Hyun, K. H. Baek, N. D. Kim, N. K. Kim, Y. N. Park, K. Song, I. Shin, *Chem. Biol.* **2015**, *22*, 391–403.
- [13] H. Yang, X. Qin, H. Wang, X. Zhao, Y. Liu, H. T. Wo, C. Liu, M. Nishiga, H. Chen, J. Ge, N. Sayed, O. J. Abilez, D. Ding, S. C. Heilshorn, K. Li, *ACS Nano* **2019**, *13*, 9880–9894.
- [14] X. Tang, L. Tan, K. Shi, J. Peng, Y. Xiao, W. Li, L. Chen, Q. Yang, Z. Qian, *Acta Pharm. Sin. B* **2018**, *8*, 587–601.
- [15] H. Gao, X. Zhang, C. Chen, K. Li, D. Ding, *Adv. Biosyst.* **2018**, *2*, 1800074.
- [16] a) B. Ouyang, F. Liu, S. Ruan, Y. Liu, H. Guo, Z. Cai, X. Yu, Z. Pang, S. Shen, *ACS Appl. Mater. Interfaces* **2019**, *11*, 38555–38567; b) J. Wu, D. H. Bremner, S. Niu, M. Shi, H. Wang, R. Tang, L. M. Zhu, *ACS Appl. Mater. Interfaces* **2018**, *10*, 42115–42126; c) P. M. Chen, W. Y. Pan, C. Y. Wu, C. Y. Yeh, C. Korupalli, P. K. Luo, C. J. Chou, W. T. Chia, H. W. Sung, *Biomaterials* **2020**, *230*, 119629.

Entry for the Table of Contents (Please choose one layout)

RESEARCH ARTICLE

The molecular motor-liked agents with excellent photothermal conversion performance, attributed from high-efficiently deactivating through nonradiative conical intersection (CI) pathway, combined with a HSP70 inhibitor for low-temperature photothermal therapy.



Jen-Shyang Ni,[†] Xun Zhang,[†] Guang Yang, Tianyi Kang, Xiangwei Lin, Menglei Zha, Yaxi Li, Lidai Wang, and Kai Li*

Page No. – Page No.

Photoinduced Nonadiabatic Decay-guided Molecular Motor Triggers Effective Photothermal Conversion for Hyperthermia Cancer Therapy